# Supporting Information

# Microstructural Analysis of Perfluoropentacene Films on Graphene and Graphite: Interface-Mediated Alignment and Island Formation

*Rocío Félix, Tobias Breuer\*, Paul Rotter, Felix Widdascheck, Bruno Eckhardt, Gregor Witte, Kerstin*

*Volz and Katharina I. Gries\**

Faculty of Physics and Materials Science Center, Philipps-Universität Marburg, 35032 Marburg, Germany

## **Content**

## 1. Description of the XRD analysis

The azimuthal orientation $\phi$ of the PFP molecules relative to the graphite lattice is derived using the following analysis:

PFP lattice planes which are not oriented parallel to the substrate planes are analyzed by rotational scans. Due to the discrete azimuthal orientation of the PFP crystallites on graphite, these planes are found only at selected, discrete positions (cf. the case of graphite SC vs. HOPG Figure 1b). The azimuthal positions of these signals in the rotational scans are then compared to the signals which correspond to the graphite "zigzag" directions. The difference between both signals is denoted as $\phi_{offset}$. Then, the relative orientation of the PFP molecules to the intersection line of the corresponding plane with the $(0\ 0\ 1)_{PFP}$ lattice plane (which lies parallel to the surface as derived from the specular XRD scans) is determined ($\phi_{axis}$). By combining these values, finally the angle between the graphite azimuths and the long molecular axis, $\phi_{eff}$, is derived.
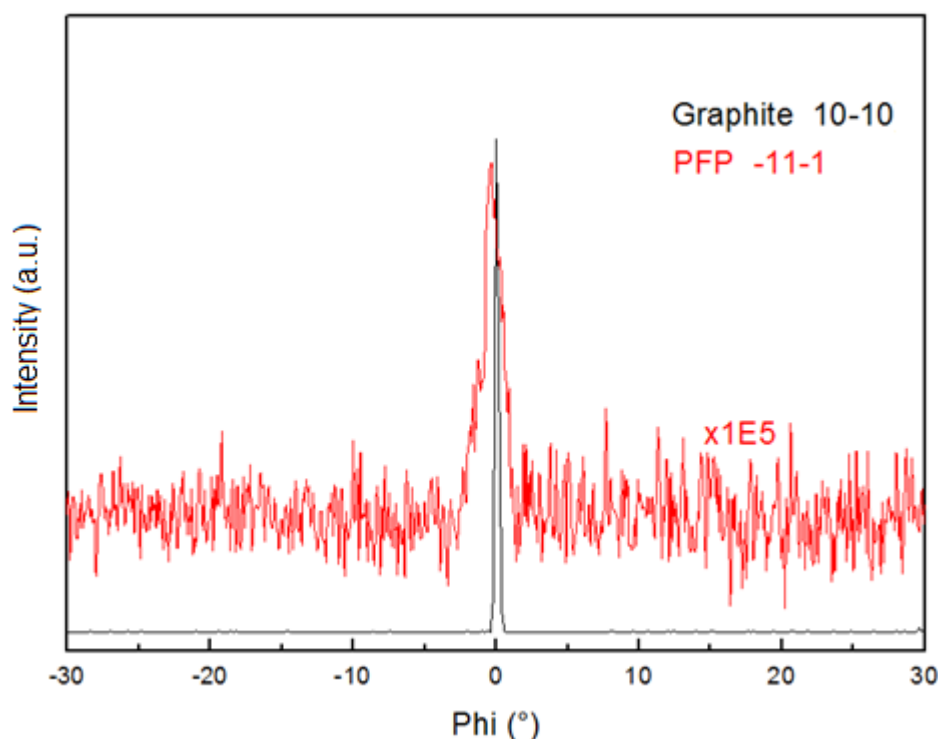
An example is provided below in Figure S1.1.



**Figure S1.1.** Rotational XRD scan of PFP on graphite.

XRD shows that the $\bar{1}\ 1\ \bar{1}_{PFP}$ signal lies at equal rotational position as the graphite $1\ 0\ \bar{1}\ 0$ signal (the corresponding normal vector lies along the "armchair" direction, cf. Figure S4). Therefore, the intersection line between the $(\bar{1}\ 1\ \bar{1})_{PFP}$ plane and the $(0\ 0\ 1)_{PFP}$ plane lies orthogonal to the "armchair" direction, i.e. parallel to the graphite "zigzag" direction (since "zigzag" direction is orthogonal to "armchair"), resulting in $\phi_{offset} = 0°$.

As shown below, the long molecular axis encloses an angle of about -3.4° with the $(\bar{1}\,1\,\bar{1})_{PFP}$ and $(0\,0\,1)_{PFP}$ plane intersection line (black dashed line in Figure S1.2), resulting in $\phi_{axis} = -3.4°$. Hence, the long axis of the molecules is rotated by $\phi_{eff} = \phi_{offset} + \phi_{axis} = -3.4°$ relative to the graphite "zigzag" direction.
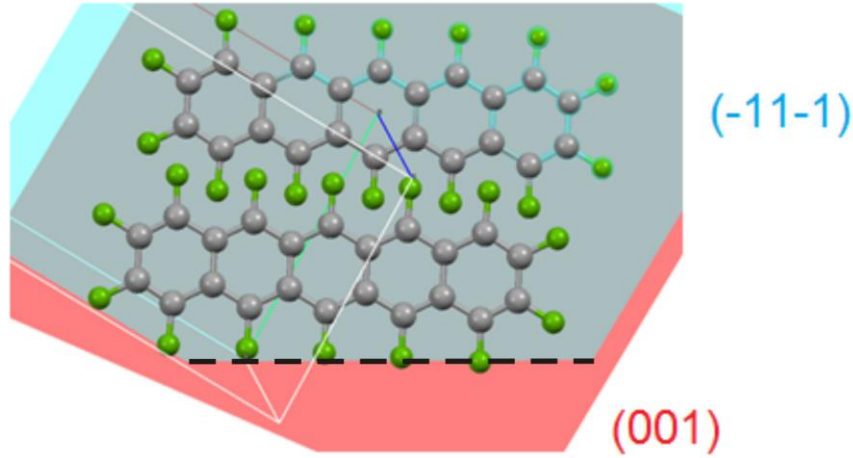


**Figure S1.2.** Visualization of the relative orientation between the long molecular axis of PFP and the intersection line of the $(0\,0\,1)$ and $(\bar{1}\,1\,\bar{1})$ planes. The black dashed line indicates their intersection line.

Furthermore, we can derive that the direction of this rotation is clockwise, i.e. the long axis encloses a negative angle with the graphite "zigzag" direction.

To provide a more accurate analysis, eight nonequivalent lattice planes have been investigated, yielding the following values for $\phi_{eff}$.

$\phi_{eff}\,(\bar{1}\,1\,\bar{1}) = -3.4°$

$\phi_{eff}\,(1\,\bar{1}\,\bar{1}) = -3.55°$

$\phi_{eff}\,(6\,0\,\bar{2}) = -4.8°$

$\phi_{eff}\,(2\,\bar{2}\,0) = -2.6°$

$\phi_{eff}\,(0\,1\,\bar{1}) = -3.8°$

$\phi_{eff}\,(4\,3\,\bar{1}) = -3.8°$

$\phi_{eff}\,(1\,1\,\bar{1}) = -3.8°$

$\phi_{eff}\,(1\,\bar{2}\,0) = -3.6°$

_____

Average: -3.67°

The related scans are provided below.

We note that some of the reflections appear twice (e.g. the 4 3 $\bar{1}$ reflex) which is due to non-equivalent positions of mirror domains resulting from the triclinic nature of the unit cell. (For example in the case of the 4 3 $\bar{1}$ reflex, the mirror domains are separated by about 19.4°, which corresponds to the observed peak splitting of about 19°.)

(a)

(b)



(c)

(d)



Graphite 10-10
PFP 2-20

x1E5

Intensitv (a.u.)

Phi (°)

(e)



Graphite 10-10
PFP 0 1-1

x1E5

Intensitv (a.u.)

Phi (°)

(f)

Graphite 10-10

PFP 43-1

Intensity (a.u.)

x1E5

-30    -20    -10    0    10    20    30

Phi (°)

(g)

Graphite 10-10

PFP 11-1

Intensity (a.u.)

x1E5

-30    -20    -10    0    10    20    30

Phi (°)
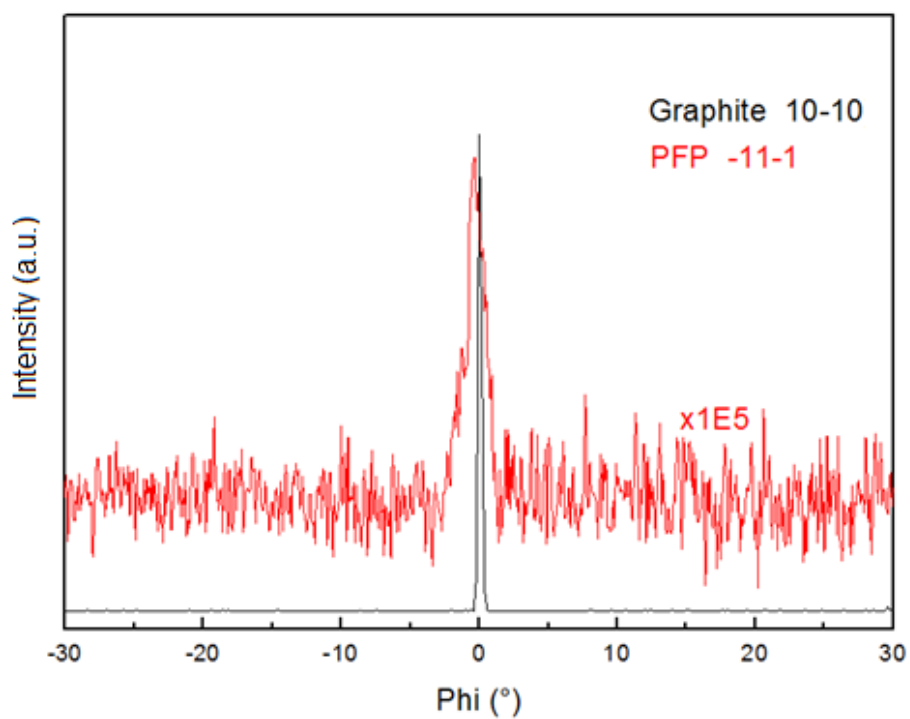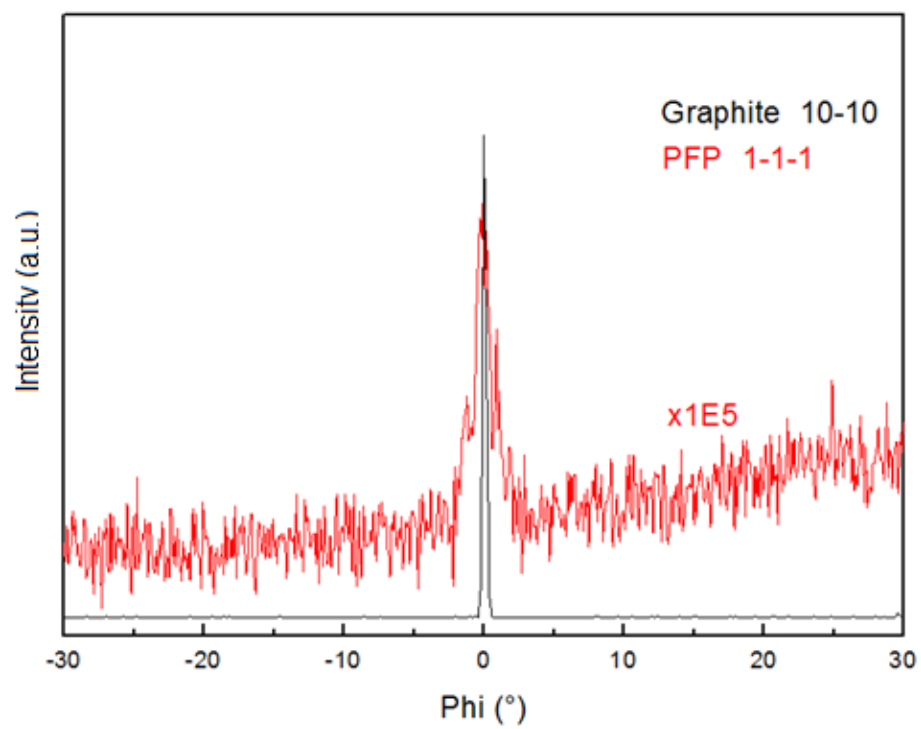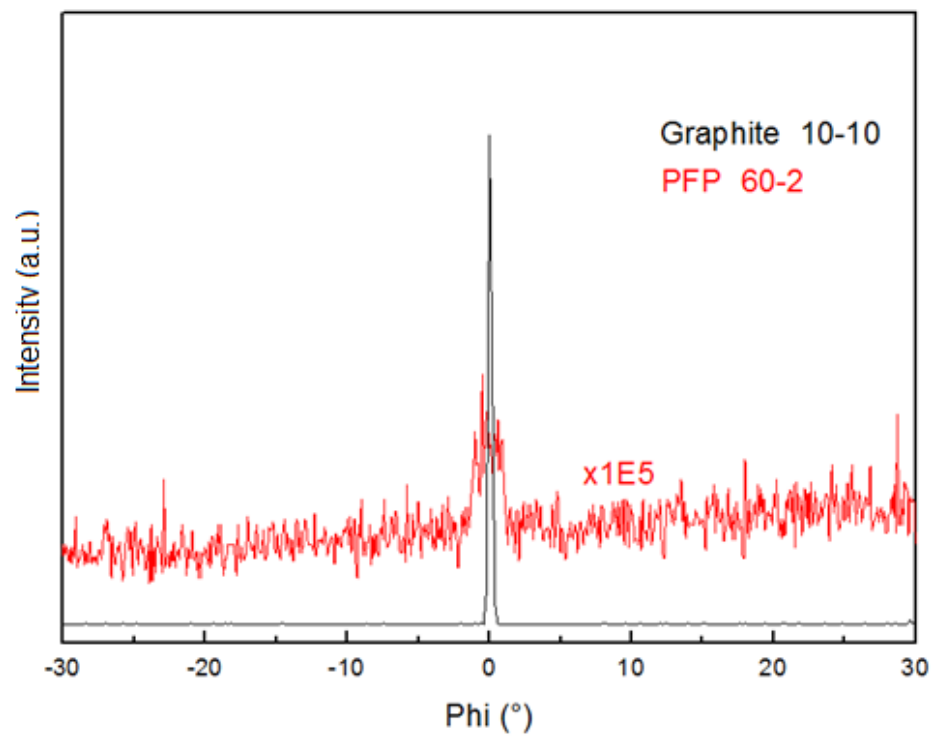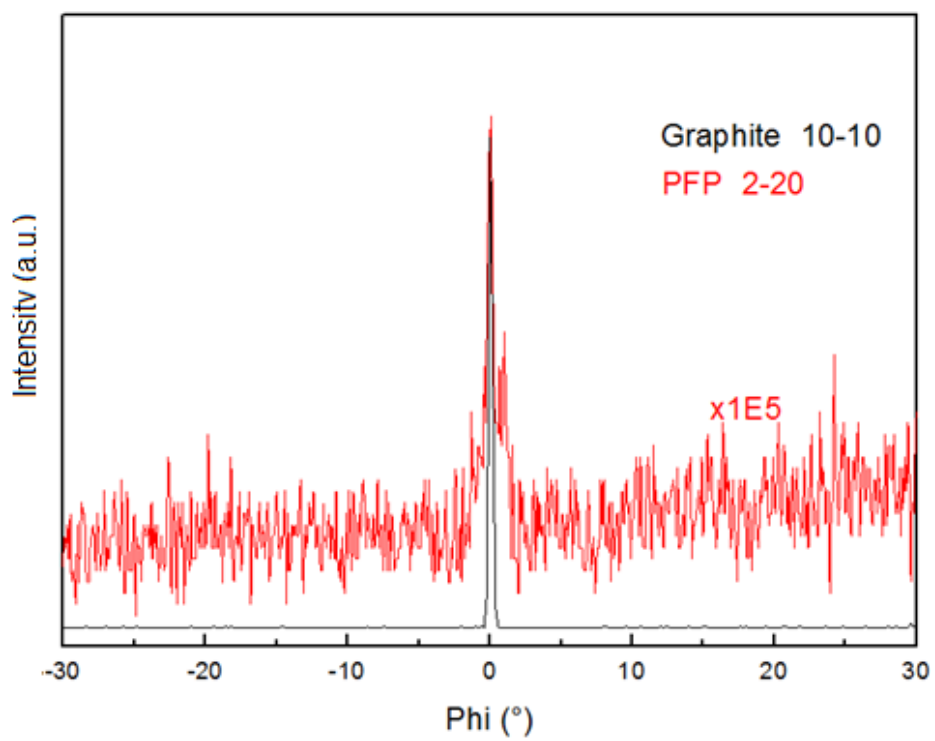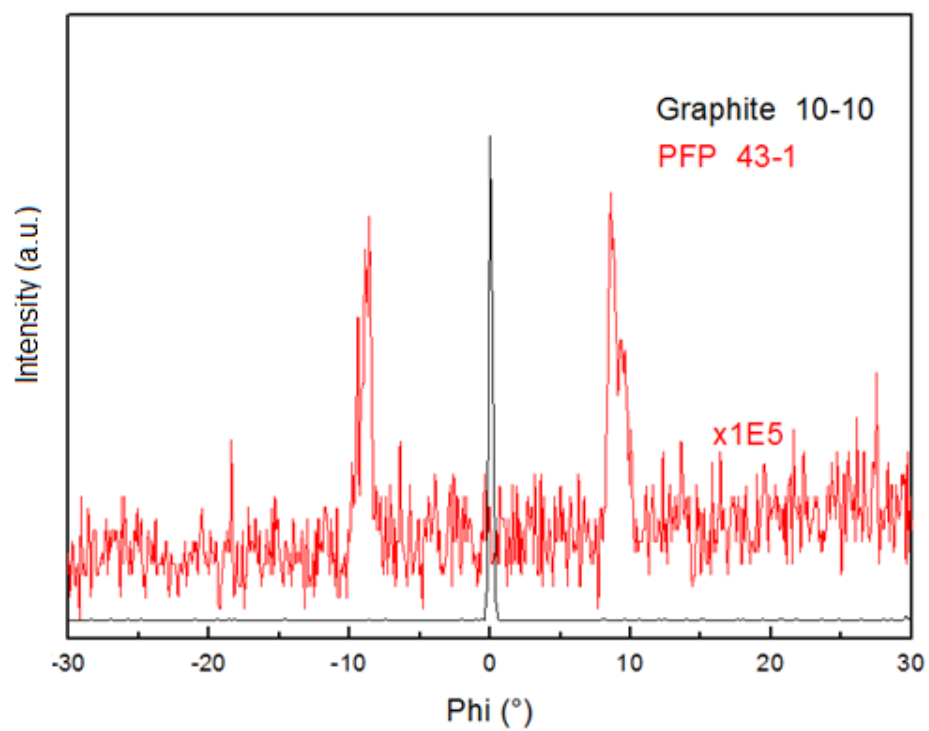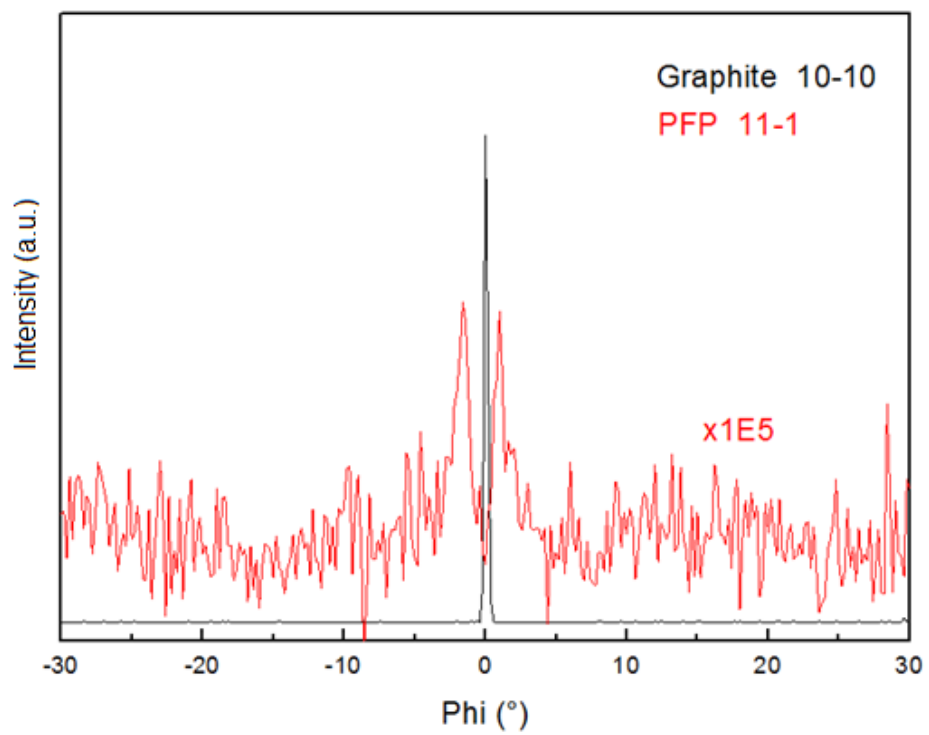
(h)
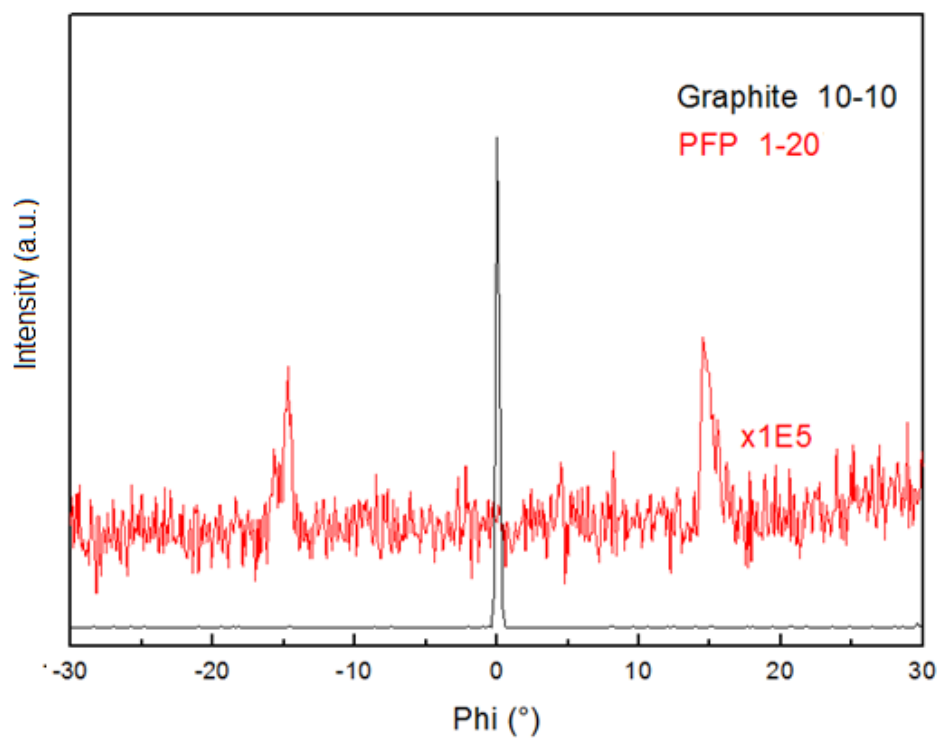


**Figure S1.3.** (a)-(h) Rotational XRD scans of PFP on graphite.

## 2. Definition of facet and edge

A definition for the used terms facet and edge has been provided in the manuscript. In Figure S2 the corresponding concepts are visualized.
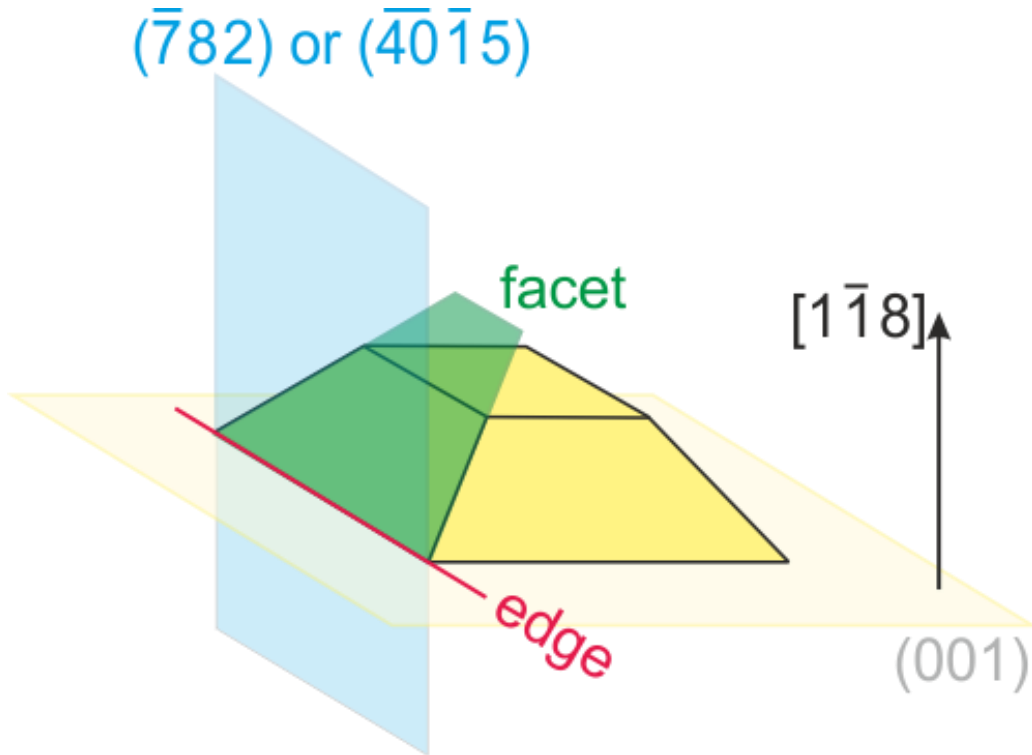


**Figure S2.** Graphical definition of the terms edge and facet. Accordingly, a facet is described by the plane which defines the real shape of an island (the inclination of the sidewall). The edge is given by the border of the PFP island that is visible in $[1\bar{1}8]$ viewing d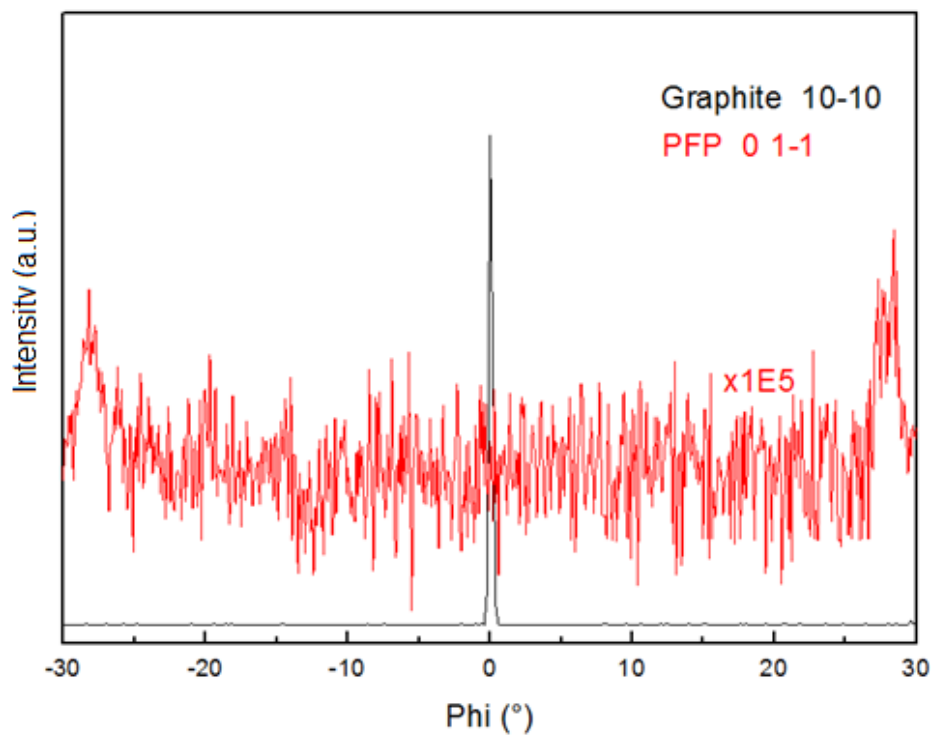irection. In addition the edge lies parallel to the intersection line of the (0 0 1) and the $(\bar{7}\,8\,2)$ or $(\overline{40}\,\bar{1}\,5)$ plane, respectively.

### 3. TEM analysis at room temperature (T ≈ 298 K)

Since a shift of the lattice parameters with the temperature has been already observed for the nonperfluorinated counterpart of PFP (pentacene, PEN) [1-3], a complementary TEM analysis was carried out at room temperature. Indeed, these measurements reveal different relative offsets between the observed PFP diffraction peaks and the graphene substrate reflections. As can be seen in Figure S3, the 11 3 $\bar{1}_{PFP}$ reflection is rotated by about -4.5° relative to the graphene reflection (enclosed in orange). This leads to an angle of approximately -3° between the long molecular axis of the PFP molecules and the graphene "zigzag" direction. In addition, the thermal expansion and contraction of the PFP crystal causes the angle between the 11 3 $\bar{1}$ and $\bar{1}$ 7 1 reflections to be smaller ($\alpha = 62°$) than the angle observed at low temperature ($\alpha = 68°$), again indicating a significant modification of the PFP crystal structure upon temperature changes. However, as can be seen in the Figure S3, the correlation between the 11 3 $\bar{1}$ and $\bar{1}$ 7 1 reflections in reciprocal space and the characteristic edges in real space still remains.
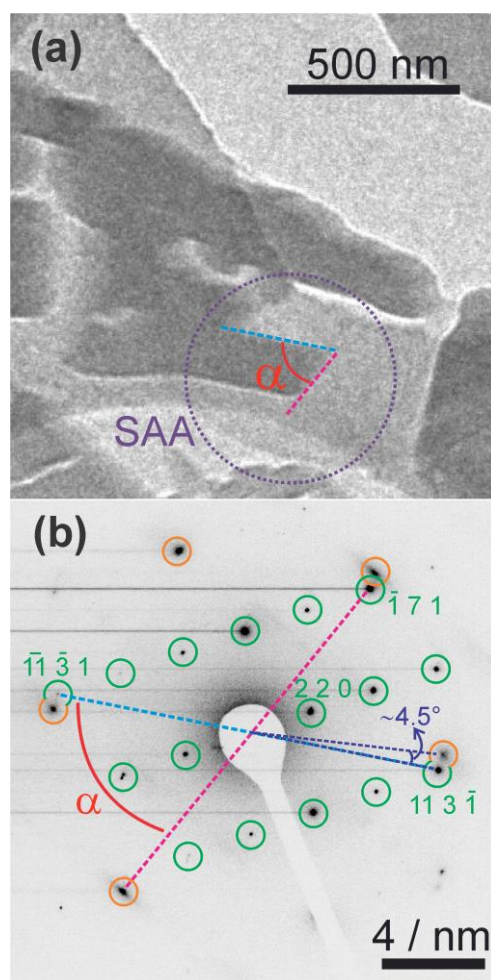


**Figure S3.** Room temperature TEM/SAED measurements. (a) BF-TEM picture of a PFP island with characteristic edges highlighted by dashed blue and pink lines. (b) SAED pattern of the region marked in (a) by the selected area diffraction aperture (SAA, dotted circle). Green circles represent the reflections for PFP while the orange circles correspond to the 1 1 $\bar{2}$ 0 graphene reflection family. The angle ($\alpha = 62°$) between the 11 3 $\bar{1}$ and $\bar{1}$ 7 1 reflections in the SAED pattern is rather similar to the angle described by the edges of the selected island. Graphene and PFP reflections enclose an angle of approximately 4.5°.

## 4. Visualization of planes and directions in PFP and graphene

The room temperature SAED pattern presented in Figure S3b showed an angle of -4.5° between the $11\,3\,\bar{1}_{PFP}$ and the $1\,1\,\bar{2}\,0_{graphene}$ reflections. In Figure S4 a sketch visualizing the rotation between the $(11\,3\,\bar{1})_{PFP}$ and the $(1\,1\,\bar{2}\,0)_{graphene}$ planes is presented. The normal to the PFP plane ($[n\,(11\,3\,\bar{1})]$) will also have a deviation of -4.5° regarding the $\langle 1\,1\,\bar{2}\,0\rangle$ "zigzag" direction of graphene. However, the vector $[n\,(11\,3\,\bar{1})]$ is not exactly parallel to the direction along the long molecular axis of the PFP molecules but exhibits an offset of approximately 1.5°. This leads to an angle of approximately -3° between the long molecular axis of the PFP molecules and the graphene "zigzag" direction.
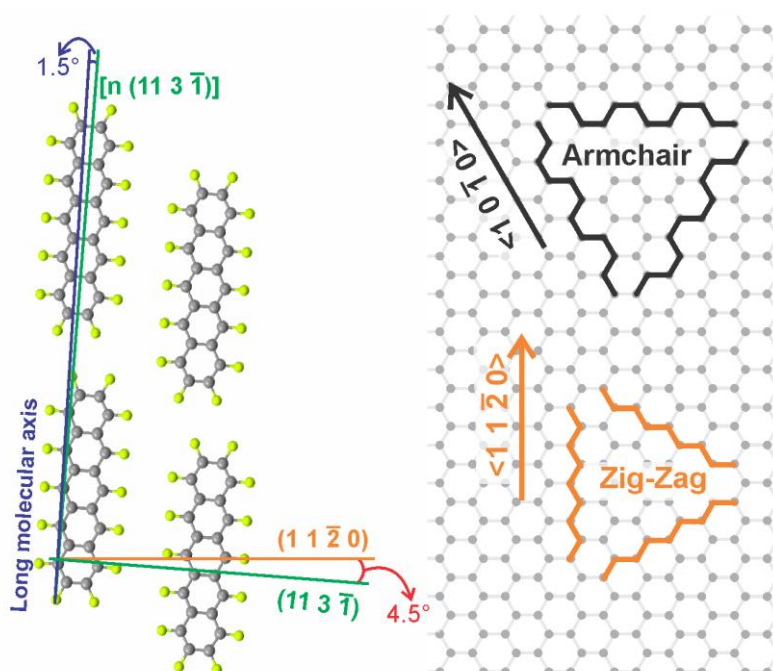


**Figure S4.** Sketch of the azimuthal orientation between the long molecular axis of PFP molecules of the bulk and the normal to the $(11\,3\,\bar{1})_{PFP}$ plane regarding the $\langle 1\,1\,\bar{2}\,0\rangle_{graphene}$ "zigzag" direction. For a better understanding, the "zigzag" and "armchair" directions of graphene have been marked in orange and black color, respectively. As can be seen the $(11\,3\,\bar{1})_{PFP}$ plane (in green) is rotated by -4.5° with respect to the $(1\,1\,\bar{2}\,0)_{graphene}$ plane (in orange). Moreover, the long molecular axis of PFP molecules (in blue) has a small offset of around 1.5° with respect to the normal of the $(11\,3\,\bar{1})_{PFP}$ plane $[n\,(11\,3\,\bar{1})]$.

## 5. Calculations of the planes lying parallel to the island edges along the $[1\,\bar{1}\,8]$ viewing direction

The correlation between the $11\,3\,\bar{1}$ and $\{\bar{1}\,7\,1\}$ reflections in reciprocal space and the characteristic confining edges in real space allows the Miller-indices determination of the planes lying parallel to the confining island edges in the $[1\,\bar{1}\,8]$ viewing direction. It has been done as follows:

While in a high symmetry system (i.e. cubic) the assignment between reflections in reciprocal space and planes in real space is simple, in a lower symmetry crystal, this procedure is more difficult. The triclinic system (angles of a unit cell are different from each other and not equal to 90°) just obeys general relations, as is the case of Weiss Zone Law [4]. This expression states that if a direction [u v w] is contained in a plane $(h\,k\,l)$, then:

$$hu + kv + lw = 0 \qquad (1)$$

In a cubic system this is exactly analogous to taking the scalar product of the direction and the plane normal. Indeed, in a cubic system, the scalar product can be used to determine the angle between a direction and a plane. However, the Weiss Zone Law is more general, and it works for all crystal systems to determine if a direction lies in a plane (including those that do not have orthogonal a, b and c axis). Given the indices of any two planes, $(h_1\,k_1\,l_1)$ and $(h_2\,k_2\,l_2)$, the indices of the [u v w] direction, in which the planes intersect, are found by solving the following equations:

$$h_1 u + k_1 v + l_1 w = 0$$
$$h_2 u + k_2 v + l_2 w = 0 \qquad (2)$$

Therefore, from the Weiss Zone Law, the common direction [u v w] between two different planes $(h_1\,k_1\,l_1)$ and $(h_2\,k_2\,l_2)$ can be derived as:

$$u = k_1 l_2 - k_2 l_1$$
$$v = l_1 h_2 - l_2 h_1 \qquad (3)$$
$$w = h_1 k_2 - h_2 k_1$$

As can be observed in Figure 5 of the paper, the drawn dotted blue and pink lines in the reciprocal space (Figure 5b), are parallel to the islands edges marked in blue and pink lines in real space (Figure 5a), respectively. Therefore, the correlation between the $11\,3\,\bar{1}_{\text{PFP}}$ and $\bar{1}\,7\,1_{\text{PFP}}$ reflections of the diffraction pattern and the island edges of the BF-TEM picture should be examined, in order to find the planes lying parallel to these island edges. In addition, it is known that the $(0\,0\,1)_{\text{PFP}}$ plane is perpendicular to the electron beam. Therefore, the Weiss Zone Law in the form of equation (3) is applied to find the common direction [u v w] between the $(11\,3\,\bar{1})$ and $(0\,0\,1)$ planes and the $(1\,\bar{7}\,\bar{1})$ and $(0\,0\,1)$ planes. These directions were calculated as $[3\,\overline{11}\,0]$ and $[\bar{7}\,\bar{1}\,0]$, respectively. Thus, $[3\,\overline{11}\,0]$ and $[\bar{7}\,\bar{1}\,0]$ directions run parallel to the intersection of the $(11\,3\,\bar{1})$ and $(0\,0\,1)$ planes and $(1\,\bar{7}\,\bar{1})$ and $(0\,0\,1)$ planes, respectively, and in turn, these directions are oriented normally to the blue and pink marked edges of Figure 5a, respectively. Thereupon, from the $[3\,\overline{11}\,0]$ and $[\bar{7}\,\bar{1}\,0]$ directions, the planes lying parallel to the blue and pink marked edges of the islands can be identified. The following equations provide the $(h\,k\,l)$ indices for these planes in the triclinic system [5]:

12

$$h = ua^2 + vab\ cos\gamma + wca\ cos\beta$$
$$k = uab\ cos\gamma + vb^2 + wba\ cos\alpha \qquad (4)$$
$$l = uca\ cos\beta + vbc\ cos\alpha + wc^2$$

Where $[u\ v\ w]$ are the indices of the direction standing normal on the $(h\ k\ l)$ plane and $a$, $b$ and $c$, and $\alpha$, $\beta$ and $\gamma$, are the unit cell parameters for the corresponding PFP unit cell. Using equation (4), normalizing the obtained values and rounding to integer values, the planes which form the edges of a PFP island were determined as $(\bar{7}\ 8\ 2)$ and $(\overline{40}\ \bar{1}\ 5)$ planes for the $[3\ \overline{11}\ 0]$ and $[\bar{7}\ \bar{1}\ 0]$ directions, respectively.

## 6. Details on the calculation method TINKER/MM3 and verification calculations

To test the suitability of TINKER and the MM3 force field for the treatment of PFP, we have performed benchmark calculations of crystal structures of related compounds. Experimentally determined structures are used as starting point and are energetically optimized with the combination TINKER/MM3. A comparison of the results with the well-known non-fluorinated pentacene allows us to check the influence of perfluorination. Finally, co-structures of perfluorinated and nonfluorinated molecules have been tested to exclude problems of describing perfluorinated conjugated structures interacting with their non-fluorinated counterparts, which constitutes our crystal structure benchmark for the adsorption of PFP on graphene.

| | pentacene Campbell phase | | pentacene Siegrist phase | |
|---|---|---|---|---|
| | exp. [6] | MM3 | exp. [7] | MM3 |
| a / Å | 7.90 | 7.78 | 6.26 | 6.26 |
| b / Å | 6.06 | 6.10 | 7.79 | 7.60 |
| c / Å | 16.01 | 15.99 | 14.51 | 14.88 |
| α / ° | 101.90 | 99.70 | 76.65 | 79.14 |
| β / ° | 112.60 | 112.38 | 87.50 | 84.02 |
| γ / ° | 85.80 | 86.49 | 84.61 | 85.78 |

| | PFP single crystal | | PS-polymoph | |
|---|---|---|---|---|
| | exp. [8] | MM3 | exp. [9] | MM3 |
| a / Å | 15.51 | 15.35 | 15.13 | 15.99 |
| b / Å | 4.49 | 4.92 | 8.94 | 9.00 |
| c / Å | 11.45 | 10.90 | 6.51 | 6.44 |
| α / ° | 90.00 | 90.00 | 78.56 | 90.17 |
| β / ° | 91.57 | 92.65 | 108.14 | 106.95 |
| γ / ° | 90.00 | 90.00 | 92.44 | 92.03 |

| | benzene/6F-benzene | | naphthalene/8F-naphthalene | |
|---|---|---|---|---|
| | exp. [10] | MM3 | exp. [11] | MM3 |
| a / Å | 9.50 | 10.09 | 7.46 | 7.08 |
| b / Å | 7.42 | 7.48 | 8.50 | 8.64 |
| c / Å | 7.53 | 7.31 | 12.71 | 13.00 |
| α / ° | 90.00 | 90.00 | 90.00 | 90.00 |
| β / ° | 95.63 | 96.47 | 99.48 | 101.26 |
| γ / ° | 90.00 | 90.00 | 90.00 | 90.00 |

**Table S6.** Calculated unit cell parameters of crystal structures (denoted as MM3) are compared with experimentally determined results from the literature (denoted as exp.). In the calculations, no restraints w.r.t. the crystal symmetry were employed.

As shown in Table S6, the experimental structures are overall well reproduced. Clearly, perfluorination does not obviate the description of conjugated molecules with MM3. In particular, different polymorphs of

pentacene and PFP are reproduced as distinct minima. We note that TINKER does not enforce the symmetry of the original crystal.

For all calculations, an interaction cutoff distance of 12 Å was used. This is feasible, because the molecules do not exhibit net dipole moments (due to being either not fluorinated or perfluorinated). Additional calculations showed that increasing the cutoff distance does not change the overall results. Considering PFP on graphene, the potential energies and their considered differences increase by 6% at most with increasing cutoff distance. However, the underlying long range remainder of the Van der Waals interaction is approximately isotropic. Therefore, the cutoff distance in particular does not influence the angular positions of the minimum configurations.

For single molecule and monolayer structure calculations an isolated PFP molecule was minimized with MM3 and then used as building block. The root mean square error of the bond lengths compared to a PFP molecule in any of the given crystal structures is smaller than 1.2%.

### 7. Thermal desorption spectroscopy

The thermal stability of the various films was characterized by thermal desorption spectroscopy (TDS), using a quadropole mass spectrometer (Balzer QMG 220) with a Feulner cup positioned close to the sample surface. The spectra were acquired by recording the mass signal of the double-charged PFP molecule ion (M++, m/z = 265 amu) during a computer-controlled linear increase of the substrate temperature from 300 to 500 K with a heating rate of $\beta = 0.5$ K/s. To provide reliable temperature measurements, a K-type thermocouple was attached directly to the sample surface.

Clearly, all spectra yield equivalent ascending flanks and the detected signal abruptly drops down at a temperature that depends on the initial film thickness. Such a behavior corresponds to multilayer desorption (zero-order kinetics). Since no additional desorption channel is observed at higher temperatures, we conclude that no stabilized monolayer is present in the films.
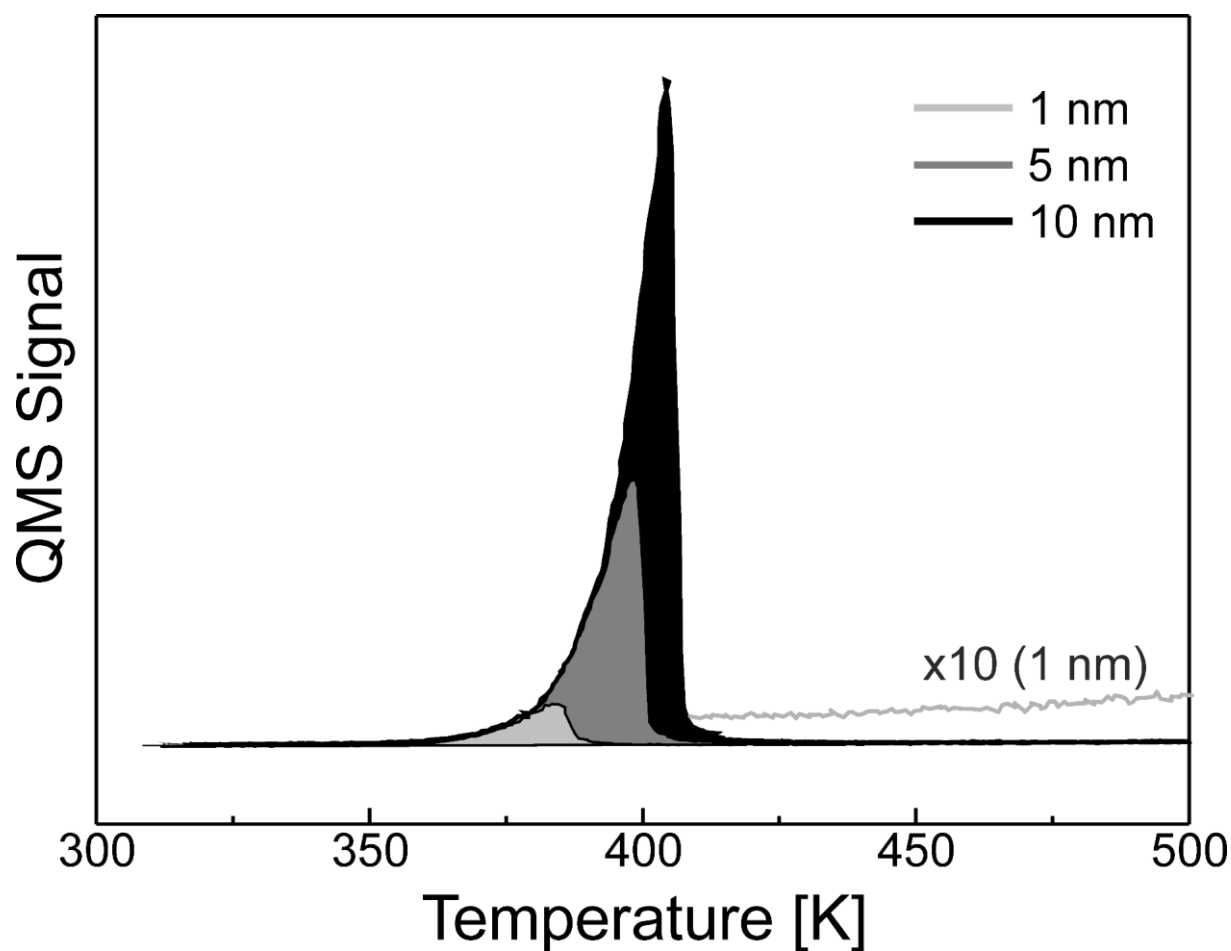


**Figure S7.** Thermal desorption spectra acquired for different thicknesses of PFP films.

## References

(1)     Mattheus, C. C.; Dros, A. B.; Baas, J.; Oostergetel, G. T.; Meetsma, A.; de Boer, J. L.; Palstra, T. T. M., Identification of polymorphs of pentacene. *Synthetic Metals* **2003,** 138, (3), 475-481.

(2)     Siegrist, T.; Besnard, C.; Haas, S.; Schiltz, M.; Pattison, P.; Chernyshov, D.; Batlogg, B.; Kloc, C., A polymorph lost and found: The high-temperature crystal structure of pentacene. *Advanced Materials* **2007,** 19, (16), 2079-2082.

(3)     Moser, A.; Novak, J.; Flesch, H.-G.; Djuric, T.; Werzer, O.; Haase, A.; Resel, R., Temperature stability of the pentacene thin-film phase. *Applied Physics Letters* **2011,** 99, (22).

(4)     Kelly, A. A.; Knowles, K. M., Crystallography and Crystal Defects, Second edition. In *Crystallography and Crystal Defects*, Sons, J. W., Ed. 2012; p 536.

(5)     Brandon, D.; Wayne, D. K., Microstructural Characterization of Materials. In *Microstructural Characterization of Materials*, Wiley, Ed. 2008; p 550.

(6)     Campbell, R. B.; Robertson, J. M.; Trotter, J., The crystal structure of hexacene, and a revision of the crystallographic data for tetracene and pentacene. *Acta Crystallographica* **1962,** 15, (3), 289--290.

(7)     Siegrist, T.; Kloc, C.; Schön, J. H.; Batlogg, B.; Haddon, R. C.; Berg, S.; Thomas, G. A., Enhanced physical properties in a pentacene polymorph. *Angewandte Chemie-International Edition* **2001,** 40, (9), 1732-1736.

(8)     Sakamoto, Y.; Suzuki, T.; Kobayashi, M.; Gao, Y.; Fukai, Y.; Inoue, Y.; Sato, F.; Tokito, S., Perfluoropentacene: High-performance p-n junctions and complementary circuits with pentacene. *Journal of the American Chemical Society* **2004,** 126, (26), 8138-8140.

(9)     Salzmann, I.; Moser, A.; Oehzelt, M.; Breuer, T.; Feng, X.; Juang, Z.-Y.; Nabok, D.; Della Valle, R. G.; Duhm, S.; Heimel, G.; Brillante, A.; Venuti, E.; Bilotti, I.; Christodoulou, C.; Frisch, J.; Puschnig, P.; Draxl, C.; Witte, G.; Muellen, K.; Koch, N., Epitaxial Growth of pi-Stacked Perfluoropentacene on Graphene-Coated Quartz. *Acs Nano* **2012,** 6, (12), 10874-10883.

(10)    Williams, J. H.; Cockcroft, J. K.; Fitch, A. N., Structure of the lowest temperature phase of the solid benzene hexafluorobenzene adduct. *Angewandte Chemie-International Edition in English* **1992,** 31, (12), 1655-1657.

(11)    Potenza, J.; Mastropaolo, D., Naphthalene-octafluoronaphthalene, 1:1 solid compound. *Acta Crystallographica Section B-Structural Science* **1975,** 31, (OCT15), 2527-2529.